

# An *in situ* and *operando* X-ray absorption spectroscopy setup for measuring sub-monolayer model and powder catalysts

Norbert Weiher,<sup>a,‡</sup> Eveline Bus,<sup>a</sup> Blazej Gorzolnik,<sup>b</sup> Martin Möller,<sup>b</sup> Roel Prins<sup>a</sup> and Jeroen Anton van Bokhoven<sup>a\*</sup>

<sup>a</sup>Institute for Chemical and Bioengineering, Swiss Federal Institute of Technology (ETH) Zurich, 8093 Zurich, Switzerland, and <sup>b</sup>Department of Textile and Macromolecular Chemistry, Institute of Technical and Macromolecular Chemistry, RWTH Aachen, 52056 Aachen, Germany.  
E-mail: j.a.vanbokhoven@chem.ethz.ch

A new spectroscopic cell has been designed for studying model catalysts using *in situ* or *operando* X-ray absorption spectroscopy. The setup allows gas treatment and can be used between 100 and 870 K. Pressures from  $10^{-3}$  Pa up to 300 kPa can be applied. Measurements on model systems in this particular pressure range are a valuable extension of the commonly used UHV characterization techniques. Using this setup, we were able to analyze the Au  $L_3$  EXAFS of a silica wafer covered with sub-monolayer concentrations of gold (0.05 ML). By modifying the sample holder, powder catalysts can also be analyzed under plug-flow conditions. As an example, the reduction of a Au/SiO<sub>2</sub> powder catalyst prepared from HAuCl<sub>4</sub> was followed.

© 2005 International Union of Crystallography  
Printed in Great Britain – all rights reserved

**Keywords:** X-ray absorption spectroscopy; *in situ*; *operando*; model catalysis; catalysis.

## 1. Introduction

Investigating the structure and chemistry of catalysts has been a central topic in science for a long time and is still a growing field of research. Studies mainly focus on the catalyst structure and its interaction with reactants, with the establishment of a structure–activity relationship being the ultimate goal (see, for example, the book chapters in Niemantsverdriet, 2000; Thomas & Thomas, 1997; van Santen, 1991; or the article by Weckhuysen, 2002). Once such a relationship is established for a given reaction, process control and further design of catalysts is feasible without costly trial-and-error approaches which are still common today. However, understanding the complex processes occurring on real catalyst surfaces is difficult because of the multitude of parameters influencing a given reaction. One way to gain more insight is by using model catalysts (Rainer & Goodman, 1998). These are well-defined systems often generated under ultrahigh vacuum (UHV) conditions whose morphology can be controlled extremely well. Preparation routes for a large variety of model systems are known and described in the literature (see, for example, Diebold, 2003; Freund *et al.*, 2003; Goodman, 2003). By means of UHV characterization techniques such as LEED, AES, XPS and FT-IR, the structure of these compounds can be resolved on the atomic scale. Preparation under UHV conditions ensures that no contaminants reside on the surface. Once

prepared, model catalysts can be exposed to low doses of reactants, typically up to  $10^{-5}$  Pa, to study their interaction and effect on the catalyst structure. These studies yield detailed insight into a particular reaction mechanism, but transferring this knowledge to real catalysis is difficult. In real catalysis, many parameters determine the operation of catalytic systems while in model studies only selected aspects are focused upon. Thus, experiments carried out in a pressure range between UHV and atmospheric pressure, using samples that have the well-defined structure of model catalysts, are extremely valuable. This approach is commonly referred to as bridging the material and pressure gaps and is a major goal in catalysis research. Bernard *et al.* used a UHV system that can be pressurized to several bars to target this problem (Bernard *et al.*, 1999). The possibility of preparing model samples under UHV conditions and subsequently pressurizing the system without exposing the sample to the atmosphere is valuable as it ensures a clean surface prior to spectroscopy.

Among other techniques such as XRD, NMR, IR and Raman spectroscopy, X-ray absorption spectroscopy (XAS) is widely applied in catalysis research. This technique yields information about the geometric and electronic structure around the absorbing atom. A single-scattering analysis of the EXAFS (extended X-ray absorption fine structure) region provides information about type, number and distance of backscattering atoms surrounding the absorber (Koningsberger *et al.*, 2000). The XANES (X-ray absorption near-edge structure) region is dominated by electronic effects

<sup>‡</sup> Current address: School of Chemical Engineering and Analytical Science, University of Manchester, Manchester M60 1QD, UK.

and multiple scattering events and thus yields information about the empty density of states in the material and the local geometry around the absorbing atom (Ankudinov *et al.*, 1998; Rehr & Ankudinov, 2005). It has been particularly useful in detecting symmetry changes by observing the violation of selection rules. XAS measurements can be performed on samples in any state of aggregation and under *in situ* or *operando* conditions such as high temperature and in the presence of a gas at high pressure. Setups exist for high and low photon energy studies (soft and hard X-rays), high (up to GPa) and low (UHV) pressures as well as for high and low temperatures (see, for example, Fulton *et al.*, 2004; Knop-Gericke *et al.*, 2000; Pascarelli *et al.*, 2004; San-Miguel *et al.*, 2000; van der Eerden *et al.*, 2000).

For catalytic studies, many setups have been designed. The groups of Lytle (Lytle *et al.*, 1979) and Koningsberger (Kampers *et al.*, 1989) presented the first cells for studying pelletized samples under flow-by conditions. Although these designs are robust and used by many groups, they have the disadvantage that the kinetic properties are not those of plug-flow reactors commonly applied to measure kinetics (Grunwaldt *et al.*, 2004). A correlation between spectroscopic and kinetic data is thus limited. Their advantage is their ease of use. The cells described by Topsøe (Clausen *et al.*, 1993) or Thomas (Sankar *et al.*, 1995) present a solution to this by placing the sample in a glass capillary at the expense of ease of use. Correlation between kinetic and spectroscopic data is often limited by the time scale of conventional EXAFS experiments. The group of Frahm developed a piezo-driven monochromator system which can record an EXAFS spec-

trum in 500 ms (see, for example, Richwin *et al.*, 2002). When the energy-dispersive detection mode is chosen, spectra can even be acquired in about 10 ms. Newton *et al.* have applied this detection mode in combination with mass spectrometry to analyze oxidation/reduction kinetics of supported Rh/Rh<sub>2</sub>O<sub>3</sub> nanoparticles (Newton *et al.*, 2005) or the interaction of NO with supported Rh<sup>I</sup>(CO)<sub>2</sub> species (Newton *et al.*, 2001).

Model catalysts are generally investigated under UHV conditions. The simultaneous acquisition of kinetic and spectroscopic data for such systems under catalytic relevant conditions is required to learn more about the active site of catalysts as well as to correlate model studies with real catalysis.

## 2. Setup description

The setup presented was designed to achieve the following: (i) to carry out model and catalytic studies in the same reactor and (ii) to investigate powder catalysts under plug-flow conditions comparable to laboratory reactors. The cell consists of a heating and cooling block as shown in Fig. 1. It is equipped with a heating cartridge which can be heated to 900 K at a maximum rate of 10 K min<sup>-1</sup> (part A). A channel in the block can be connected to a line containing liquid nitrogen or any other cooling device (part C). The lowest temperature achievable is 100 K. The temperature is measured using a NiCr/Ni thermocouple mounted directly below the sample surface. For model studies, the gas inlet is located in the window system and described in the corresponding section (Fig. 2, part C). Two gas outlets placed at the back of the block (part B) ensure a symmetric gas flow. To minimize thermal loss, the block is isolated with quartz wool. Part D is hollow to allow for water cooling of the window. The cell is mounted on

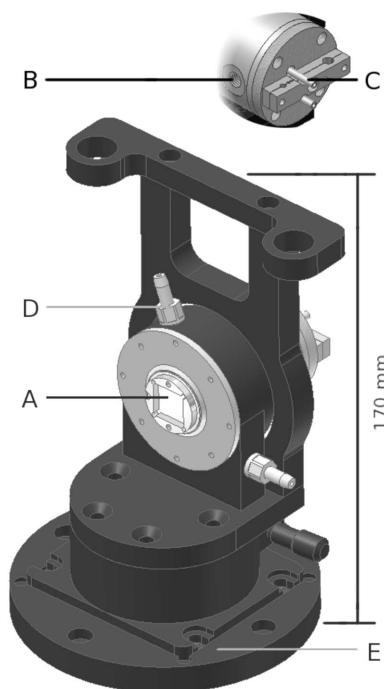


**Figure 1**  
Heating block of the XAS cell. The upper part of the figure is a view from the back. A: heating cartridge with thermocouple; B: gas outlets (for model studies); C: sample cooling; D: window cooling for high-temperature operation; E: rotation stage for cell alignment.

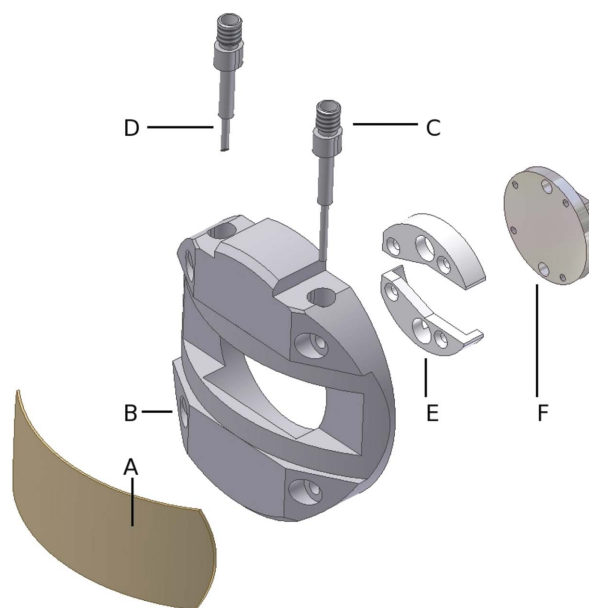


**Figure 2**  
Cell configuration for model catalyst studies. A: Kapton window; B: window frame; C: gas inlet nozzle; D: connection for mass spectrometer; E: sample fixation ceramics; F: sample support plate.

a rotating table (Newport, part E). By adjusting the angle between sample, beam and detector, grazing-incidence as well as grazing-exit measurements can be performed if necessary. The center of the sample is always located in the center of the beam.

Fig. 2 shows the sample holder used for model studies. The model catalysts are wafers of dimensions  $15\text{ mm} \times 15\text{ mm} \times 2\text{ mm}$  and are fixed on an aluminium holder (part F) using two ceramic fittings (part E). Aluminium is used to avoid X-ray scattering and undesired X-ray fluorescence radiation if synchrotron radiation hits any part of the cell. The cell is sealed with a window frame (part B) using Kapton foil (part A). The gas inlet nozzle (part C) distributes the gas over the surface. The shape of the fixating ceramics forces the gas to flow over the sample. A capillary is positioned above the sample surface (part D) for probing the gas composition with either a mass spectrometer or a gas chromatograph. After passing the gas probe, the gas flows to the back end of the cell where the outputs are located (Fig. 1, part B). The design is characterized by small dead volume, symmetric gas flow and a gas probe connection close to the sample surface which is necessary for detecting changes in the gas composition during the reaction. All gas connections are built with standard Swagelok 1/16" tubes and fittings.

Fig. 3 shows the configuration for kinetic experiments under plug-flow conditions. Catalysts are sieved to the desired grain size and inserted into the reactor (part C) equipped with a gas inlet and outlet (part D). A hole directly below the catalyst bed provides space for a thermocouple to additionally control the sample temperature. The size and shape of the engraving containing the sample can be tuned. Its width and height are chosen to match the beam configuration of most beamlines and the required dimensions of specific catalytic conditions ( $18\text{ mm} \times 2\text{ mm} \times 2\text{ mm}$ ). Sample amounts between 50 and 200 mg can be dealt with. The reactor is sealed either with Al ( $d = 10\text{ }\mu\text{m}$ ) or Teflon foil ( $d = 50\text{ }\mu\text{m}$ ; part A) using a window seal (part B). It is mounted on the heating block, and tubings for gas inlet and outlet are connected.

The separation of sample holder and heating block gives a high flexibility with respect to adapting the cell to special experimental needs. The reactor can be used for powder and model catalyst studies using the fluorescence detection mode.

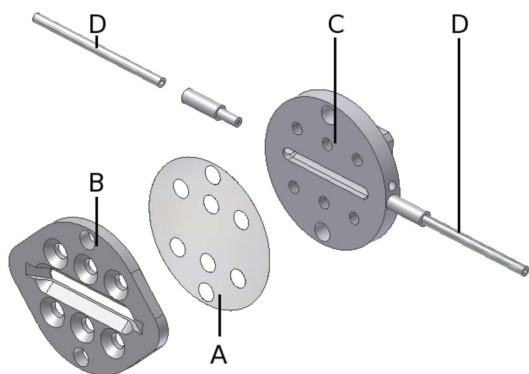


**Figure 3**  
Cell configuration for powder catalyst studies. A: X-ray transparent window; B: window seal; C: sample holder; D: gas connections.

A modification for measuring the XAS of pelletized samples under flow-through conditions in transmission and fluorescence mode is planned.

The cell has been found to work reliably in the pressure range between  $10^{-3}\text{ Pa}$  and 300 kPa at temperatures between 100 and 900 K. Compared with the earlier designs mentioned in the *Introduction*, the cell has gas flow characteristics which are similar to standard laboratory plug-flow systems. Using a mass spectrometer or gas chromatograph, kinetic data can be acquired throughout the spectroscopic experiments. Compared with the capillary setups mentioned in the *Introduction*, the main advantage is its ease of use. No fragile parts are involved in our cell.

### 3. Exemplary studies

#### 3.1. Sub-monolayer model catalysts

Arrays of nano-sized Au clusters on  $\text{SiO}_2$  wafers were prepared by means of self-assembly of diblock copolymers into reverse micelles in a non-polar solvent (Spatz, Mossmer & Möller, 1996; Spatz, Roescher & Möller, 1996). Micelles were formed using poly[isoprene(775)]-block-poly[2-vinylpyridine(565)]. They were loaded with gold salt using molar ratios of 0.3 and 0.1 between gold and diblock copolymer and supported on the wafers by dip-coating.  $\text{H}_2$  plasma was used to remove the polymer matrix and reduce the gold salt. The wafers were sized  $15\text{ mm} \times 15\text{ mm} \times 2\text{ mm}$  and had a gold coverage of 0.05 and 0.3 monolayers. The coverage was estimated from atomic force microscopy (AFM) and scanning electron microscopy (SEM) pictures (see below). X-ray photoelectron spectroscopy (XPS) proved the metallic state of the particles for both coverages. For the coverage of 0.3 monolayers (ML), AFM showed a particle height of 6 nm with an interparticle distance of 55 nm. For the coverage of 0.05 ML, a combination of AFM and SEM showed pancake-shaped particles with a height of 2.5–3.5 nm and an interparticle distance of 55 nm. All XAS studies were carried out at the ID26 beamline of the European Synchrotron Radiation Facility (ESRF). Spectra were recorded in fluorescence mode using a 13-element germanium detector. A sufficient signal-to-noise (S/N) ratio for analyzing the EXAFS region was achieved within 8 h of measurement per spectrum. Each sample was measured under the following conditions: (a) in a He flow at  $20\text{ ml min}^{-1}$  at room temperature (RT), and (b) in a flow of 4%  $\text{H}_2/\text{He}$  at  $20\text{ ml min}^{-1}$  at RT after treatment with the same gas composition at 373 K for 1 h.

Fig. 4 shows the Au  $L_3$ -edge XANES region along with the  $k^2$ -weighted EXAFS (inset). The XANES region of all four spectra shows the following features which are typical of bulk gold: an inflection point (edge position) at 11919 eV, a shoulder at 11930 eV and two characteristic peaks at 11947 and 11970 eV. The sample with high gold coverage shows a high S/N ratio which is significantly lower in the case of the lower coverage after the same scanning time. Some points were removed from the spectra (0.3 ML coverage: around 11930 eV; 0.05 ML: around 11920 and 11980 eV). This was

**Table 1**

EXAFS fits for the investigated samples (*cf* Figs. 4 and 5).

The fits have been performed in *R*-space using Hanning windows. Fitting parameters for the model catalysts are  $\Delta k$ : [2.8:8] Å<sup>-1</sup>,  $\Delta R$ : [1.5:3.5] Å,  $N_{\text{ind}}$ : 6.5,  $N_{\text{par}}$ : 4. In the case of the powder catalyst, these values are  $\Delta k$ : [3:8.5] Å<sup>-1</sup>,  $\Delta R$ : [1:4] Å,  $N_{\text{ind}}$ : 8,  $N_{\text{par}}$ : 4. For spectra A, B and E, the errors are  $\pm 10\%$ . Owing to the poor S/N ratio in case of spectra C and D, the errors increase to  $\pm 30\%$ .  $S_0^2$  has been kept fixed to the value obtained for bulk Au foil (0.83).

Sample, condition	<i>N</i>	<i>R</i> (Å)	$\sigma^2$ (Å <sup>2</sup> )	<i>E</i> <sub>0</sub> (eV)	<i>R</i> -factor
0.3 ML, He [A]	11.4	2.85	0.009	4.45	0.02
0.3 ML, H <sub>2</sub> [B]	11.5	2.85	0.010	4.61	0.01
0.05 ML, He [C]	11.0	2.87	0.009	5.11	0.20
0.05 ML, H <sub>2</sub> [D]	10.9	2.86	0.010	6.68	0.13
Au/SiO <sub>2</sub> , 1 wt%, He [E]	6.4	2.83	0.010	5.21	0.03

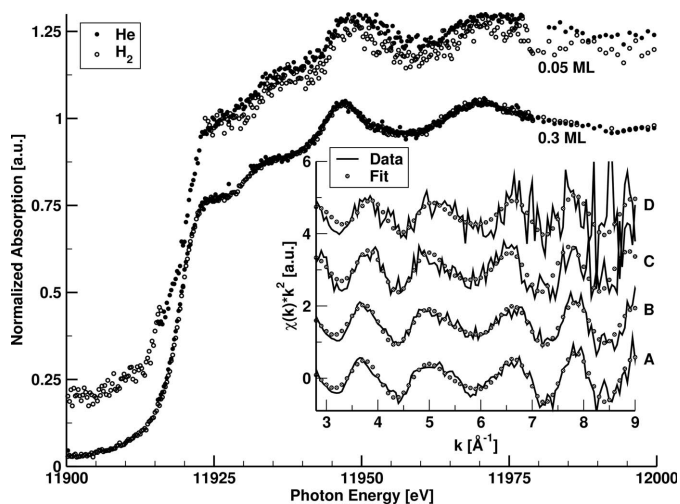


**Figure 4**  
XANES and  $k^2$ -weighted EXAFS (inset) of the model catalyst samples. Spectra in the inset correspond to: (A) 0.3 ML, He, (B) 0.3 ML, H<sub>2</sub>, (C) 0.05 ML, He and (D) 0.05 ML, H<sub>2</sub>.

necessary because the data contained glitches at these energy positions caused by Bragg reflections from the support. Their position could be varied by rotating the cell by tenths of a degree. We tried to optimize the sample position in all cases, but did not succeed in removing all glitches from the data range of interest. The EXAFS region (inset, Fig. 4) is dominated by Au–Au backscattering. The EXAFS analysis (Table 1) shows for all model catalysts a coordination number (CN) of 11, a nearest-neighbour distance of 2.86 Å, an  $E_0$  value of 5.21 eV and a Debye–Waller factor of 0.0095 Å<sup>2</sup>. The value for  $S_0^2$  (0.83) has been kept fixed at the value obtained in a fit of Au foil with a CN of 12. The slight deviation between the fits of the model catalysts is below the statistical significance of  $\pm 10\%$  for the high and  $\pm 30\%$  for the low coverage. The poorer *R*-factors of the fits of the sample with low gold coverage are caused by the poorer S/N ratio. While spectra of the high coverage sample could be fitted by freely varying all parameters, the samples with a low coverage needed a step-wise approach by fitting each parameter independently. An examination of the fit statistics yielded a much flatter parameter surface. This manifests itself as less pronounced changes in the *R*-factor when varying a given parameter as well as in high correlation between parameters. These data show that

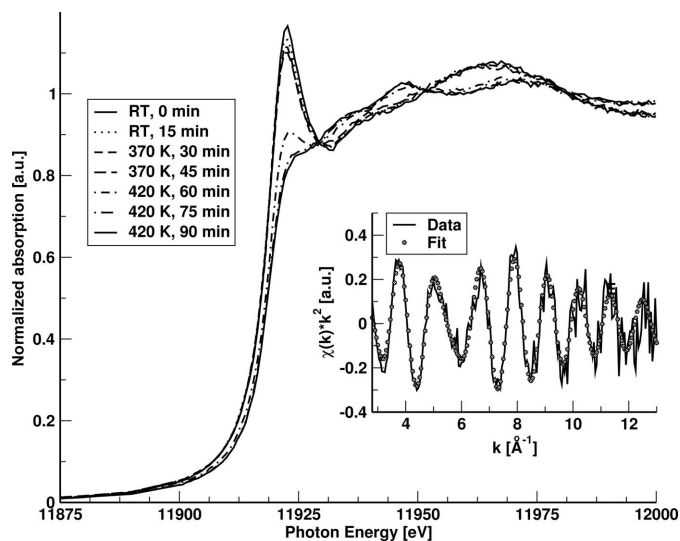


**Figure 5**  
XANES and  $k^2$ -weighted EXAFS (inset) of the Au/SiO<sub>2</sub> catalyst (E) during reduction and in He.

the Au *L*<sub>3</sub> EXAFS region of supported gold model catalysts with sub-monolayer coverage can be measured and analyzed while varying gas composition and temperature.

### 3.2. Reduction of a powder Au/SiO<sub>2</sub> catalyst

Au/SiO<sub>2</sub> was prepared by incipient wetness impregnation of the support with an aqueous solution of HAuCl<sub>4</sub>. After impregnation, the sample was washed using aqueous ammonia and deionized water and dried under vacuum at room temperature for 2 h. All data were recorded at the ESRF, beamline BM01B, using a 13-element Ge detector for acquiring the fluorescence XAS spectra. Owing to the higher gold content of 1 wt%, an acceptable S/N ratio could be achieved within 2 h per EXAFS spectrum and within 15 min per XANES spectrum. The XANES region of the sample in He at RT (Fig. 5) showed an edge position of 11917 eV, a sharp white line at 11923 eV, a minimum at 11932 eV and a broad peak at 11966 eV. These features are usually observed for gold in an oxidation state of 3+, such as AuCl<sub>3</sub> and Au<sub>2</sub>O<sub>3</sub>. A reduction was carried out to compare this sample with the model systems described above. The sample was heated in 5% H<sub>2</sub>/He using a heat rate of 5 K min<sup>-1</sup> until reduction was complete. The catalyst was fully reduced at 420 K. The characteristic XANES features mentioned above for Au<sup>0</sup> (edge position: 11919 eV, features at 11930, 11947 and 11970 eV) were clearly visible after this treatment. Afterwards, hydrogen was removed by flowing He at 420 K over the sample for half an hour. After cooling to room temperature, EXAFS spectra were recorded. All XANES features of the powder catalyst were damped and broadened when compared with the features of the model samples. The EXAFS region is again dominated by the Au–Au backscattering. The  $E_0$  and  $\sigma^2$  values obtained for the powder sample are identical to those obtained for the model catalysts. The CN of 6.4 indicates a particle diameter of  $\sim 8$  Å. The differences in the first-shell distance between model samples (average 2.86 Å) and powder

catalyst (2.83 Å) are on the border of statistical significance. However, a contraction in the Au–Au distance of such small particles is expected (Apai *et al.*, 1979; Boswell, 1951; Delley *et al.*, 1983).

### 3.3. Interpretation

For the model catalysts (spectra A–D) we find that the EXAFS parameters are typical for a system containing metallic bulk Au<sup>0</sup>: a CN close to 12, a nearest-neighbour distance close to the value of gold foil (2.88 Å), reasonable  $E_0$  shifts ( $4 < E_0 < 7$  eV) and Debye–Waller factors. The poorer S/N ratio in the case of the low gold coverage complicates the fitting process but does not hinder data interpretation significantly. The XANES region additionally supports this electronic and geometric structure: all features characteristic for Au<sup>0</sup> are present with no significant differences between spectra A–D. Model calculations using *FEFF8* (Ankudinov *et al.*, 1998) showed that changes in  $R$  and  $E_0$  influence the feature positions in XANES and EXAFS while changes in  $N$  and the Debye–Waller factor dampen and broaden the features.

There are, however, significant differences between the flat supported model catalysts and the powder catalyst (spectra A–D and E). The oxidation state of the gold atoms prior to any treatment is 3+ (spectrum E) and 0 (spectra A–D). Upon reduction of the powder Au/SiO<sub>2</sub> catalyst, the characteristic features of Au<sup>0</sup> become visible. The spectra recorded during the reduction process (Fig. 5) show three isobestic points at 11930, 11951 and 11980 eV, which point to a transition from Au<sup>3+</sup> to Au<sup>0</sup> without passing through an intermediate state like Au<sup>+</sup> or Au<sup>2+</sup>. After reduction, the powder catalyst has a significantly lower CN than the model catalysts. The value of 6.4 corresponds to a particle size of ~8 Å. The broadened XANES features additionally support this observation. The nearest-neighbour distance indicates a contraction of the particles compared with bulk Au which is in line with the literature (Apai *et al.*, 1979; Boswell, 1951; Delley *et al.*, 1983).

### 4. Conclusions

We have designed a setup for studying well defined model compounds under catalytic relevant conditions. The setup is flexible and enables measurement of powders and pellets, including transmission and electron yield detection by small modifications of the sample holder. The two main advantages are the possibilities (i) to study model systems like well-defined particles on oxidic wafers under the same conditions as real catalytic samples and (ii) to study a catalytic reaction spectroscopically and kinetically in the same setup. It thus facilitates data correlation between model catalysis and real catalysis as well as between kinetic and spectroscopic studies. The examples presented show the data quality obtained for coverages as low as 0.05 monolayers using a near-grazing-incidence configuration.

We thank the ESRF for providing beam time at stations ID26 and BM01B as well as the station scientists (O. Safonova, H. Emerich, W. van Beek) for their support. This project has been supported by the Swiss National Fonds and the European Union under contract No. HPRN-1999-00151.

### References

- Ankudinov, A. L., Ravel, B., Rehr, J. J. & Conradson, S. D. (1998). *Phys. Rev. B*, **58**, 7565–7576.
- Apai, G., Hamilton, J. F., Stohr, J. & Thompson, A. (1979). *Phys. Rev. Lett.* **43**, 165–169.
- Bernard, P., Peters, K., Alvarez, J. & Ferrer, S. (1999). *Rev. Sci. Instrum.* **70**, 1478–1480.
- Boswell, F. W. C. (1951). *Proc. Phys. Soc. London A*, **64**, 465–475.
- Clausen, B. S., Grabaek, L., Steffensen, G., Hansen, P. L. & Topsøe, H. (1993). *Catal. Lett.* **20**, 23–36.
- Delley, B., Ellis, D. E., Freeman, A. J., Baerends, E. J. & Post, D. (1983). *Phys. Rev. B*, **27**, 2132–2144.
- Diebold, U. (2003). *Surf. Sci. Rep.* **48**, 53–229.
- Eerden, A. M. J. van der, van Bokhoven, J. A., Smith, A. D. & Koningsberger, D. C. (2000). *Rev. Sci. Instrum.* **71**, 3260–3266.
- Freund, H. J., Baumer, M., Libuda, J., Risse, T., Rupprechter, G. & Shaikhutdinov, S. (2003). *J. Catal.* **216**, 223–235.
- Fulton, J. L., Chen, Y., Heald, S. M. & Balasubramanian, M. (2004). *Rev. Sci. Instrum.* **75**, 5228–5231.
- Goodman, D. W. (2003). *J. Catal.* **216**, 213–222.
- Grunwaldt, J. D., Caravati, M., Hannemann, S. & Baiker, A. (2004). *Phys. Chem. Chem. Phys.* **6**, 3037–3047.
- Kampers, F. W. H., Maas, T. M. J., van Grondelle, J., Brinkgreve, P. & Koningsberger, D. C. (1989). *Rev. Sci. Instrum.* **60**, 2635–2638.
- Knop-Gericke, A., Havecker, M., Schedel-Niedrig, T. & Schlögl, R. (2000). *Top. Catal.* **10**, 187–198.
- Koningsberger, D. C., Mojet, B. L., van Dorssen, G. E. & Ramaker, D. E. (2000). *Top. Catal.* **10**, 143–155.
- Lytle, F. W., Wei, P. S. P., Greigor, R. B., Via, G. H. & Sinfelt, J. H. (1979). *J. Chem. Phys.* **70**, 4849–4855.
- Newton, M. A., Burnaby, D. G., Dent, A. J., Diaz-Moreno, S., Evans, J., Fiddy, S. G., Neisius, T., Pascarelli, S. & Turin, S. (2001). *J. Phys. Chem. A*, **105**, 5965–5970.
- Newton, M. A., Fiddy, S. G., Guilera, G., Jyoti, B. & Evans, J. (2005). *Chem. Commun.* **1**, 118–120.
- Niemantsverdriet, J. W. (2000). *Spectroscopy in Catalysis – An Introduction*. Weinheim: Wiley-VCH.
- Pascarelli, S., Mathon, O. & Aquilanti, G. (2004). *J. Alloy Compd.* **362**, 33–40.
- Rainer, D. R. & Goodman, D. W. (1998). *J. Mol. Catal. A*, **131**, 259–283.
- Rehr, J. J. & Ankudinov, A. L. (2005). *Coord. Chem. Rev.* **249**, 131–140.
- Richwin, M., Zaeper, R., Lützenkirchen-Hecht, D. & Frahm, R. (2002). *Rev. Sci. Instrum.* **73**, 1668–1670.
- Sankar, G., Thomas, J. M., Rey, F. & Greaves, G. N. (1995). *J. Chem. Soc. Chem. Commun.* **24**, 2549–2555.
- San-Miguel, A., Pellicer-Porres, J., Segura, A., Itie, J. P., Polian, A. & Gauthier, M. (2000). *High Press. Res.* **19**, 725–730.
- Santen, R. A. van (1991). *Theoretical Heterogeneous Catalysis*. Singapore: World Scientific.
- Spatz, J. P., Mossmer, S. & Möller, M. (1996). *Chem. Eur. J.* **2**, 1552–1555.
- Spatz, J. P., Roescher, A. & Möller, M. (1996). *Adv. Mater.* **8**, 337–340.
- Thomas, J. M. & Thomas, W. J. (1997). *Principles and Practice of Heterogeneous Catalysis*. Weinheim: VCH.
- Weckhuysen, B. M. (2002). *Chem. Commun.* **58**, 97–110.